coatings

MDPI

Article

Thermal-Mechanical Coupling Analysis of Permeable Asphalt Pavements

Yuekun Li [1], Xulong Wang [2], Hailong Zhang [2], Zhenxia Li [2,3,4,*] and Tengteng Guo [2,3,4]

[1] College of Geosciences and Engineering, North China University of Water Resources and Electric Power, Zhengzhou 450046, China
[2] School of Civil Engineering and Transportation, North China University of Water Resources and Electric Power, Zhengzhou 450045, China
[3] Henan Province Engineering Technology Research Center of Environment Friendly and High-Performance Pavement Materials, Zhengzhou 450045, China
[4] Zhengzhou City Key Laboratory of Environmentally Friendly High Performance Road and Bridge Materials, Zhengzhou 450045, China
* Correspondence: zhenxiali2009@ncwu.edu.cn

Abstract: In order to clarify the mechanical response of permeable asphalt pavements under a temperature effect, the mechanical responses of different types of permeable asphalt pavements, which were based on a self-developed drainage SBS-modified asphalt mixture with fiber, were simulated using ANSYS finite element software (APDL 19.2). The influence of temperature and temperature change on the mechanical behavior of the permeable asphalt pavements was studied, and the mechanical responses of the pavements at different driving speeds was analyzed. The results show that the extreme values of surface deflection, compressive strain of the soil foundation top surface, and the shear stress and tensile stress of the upper-layer bottom of the three kinds of pavements under dynamic load were about 10% smaller than those under static loads, and the extreme values under different temperature conditions were 28%~50% larger than the values obtained without different temperature conditions. During the 12 h heating process, the mechanical indexes of the three types of pavements with axle loads were consistent with the change law of temperature, and the peak values of the mechanical indexes under dynamic loads were smaller than those under static loads. In addition, the mechanical indexes of the three types of pavements under dynamic loads had the same law of change with speed under the same conditions, and the values were less than the extreme values under static loads, but the degree of influence was different.

Keywords: permeable asphalt pavement; temperature effect; mechanical response; finite element simulation

Citation: Li, Y.; Wang, X.; Zhang, H.; Li, Z.; Guo, T. Thermal-Mechanical Coupling Analysis of Permeable Asphalt Pavements. *Coatings* **2024**, *14*, 582. https://doi.org/10.3390/coatings14050582

Academic Editor: Valeria Vignali

Received: 31 March 2024
Revised: 3 May 2024
Accepted: 4 May 2024
Published: 7 May 2024

1. Introduction

With the rapid development of the economy and the acceleration of urban construction, the natural ground in cities gradually becomes covered by impervious hardened surfaces. These surfaces have good bearing capacity and aesthetics but also bring some negative effects to the urban ecological environment [1–3]. Permeable Asphalt Concrete (PAC), a new type of pavement structure based on the green sponge city concept, is widely used because of its good skid resistance, noise reduction and water permeability properties [4,5].

Because porosity is the key factor affecting the permeability of a pavement, the permeability coefficient of the pavement is mainly affected by the connected pores of the material, and the connected pores are closely related to the composition of the material and the shape of the aggregate. Therefore, researchers have conducted much research on the material composition of pavements. Scholars often use the porosity and permeability of a permeable asphalt pavement as the key indicators of pavement design. Considering the relationship between the porosity of a permeable asphalt pavement and the key sieve

holes, the key sieve hole affecting the porosity of the mixture has a passing rate of 2.36 mm. Careful design to achieve passing rates of 4.75 mm and 2.36 mm allows the mixture to more easily form a skeleton structure [6–8]. The porosity of a permeable asphalt mixture affects the high-temperature stability, low-temperature deformation resistance and water damage resistance. Under the same thermal aging time, there is a positive linear relationship between dynamic stability and porosity. However, the higher the porosity of a porous asphalt mixture, the higher the tendency for flexural tensile failure and shrinkage stress at low temperature, and the worse the ability to resist water damage [9]. At the same time, researchers have found that under the same rainfall conditions, there is not only a good linear correlation between porosity and the permeability coefficient, but also a correlation between surface thickness and the permeability coefficient. In addition, the increase in porosity and pavement thickness can not only effectively improve the drainage effect of pavements, but also improve the water storage capacity of permeable roads. A greater total thickness of pavement, especially with an increase in porosity from 18% to 22%, can significantly improve the water storage capacity of permeable roads [10].

Permeable asphalt pavements are widely used in high-rainfall areas because of their high permeability. Therefore, some researchers have studied the permeability and road performance of pavement structures. The skid resistance of a drainage asphalt mixture is easily affected by rainfall conditions. From the analysis of the relationship between surface characteristics and skid resistance, it can be seen that with an increase in rainfall, the friction coefficient of a drainage asphalt mixture decreases rapidly and then tends to be stable [11]. During a rainfall event, the runoff coefficient of a permeable asphalt pavement is a single-peak dynamic change, and when the rainfall intensity is less than 50 mm/h, the permeable asphalt pavement does not produce runoff [12]. The cross slope and the longitudinal slope have significant effects on the drainage performance of the porous asphalt surface layer. The improvement in the drainage performance resulting from the cross slope is affected by the size of the longitudinal slope, and the thickness and width of the pavement. The influence of the longitudinal slope change decreases with the increase in the percentage of the cross slope and the decrease in the ratio of the thickness of the porous asphalt layer to the width of the pavement [13]. The influence of the road surface on rainwater runoff is mainly affected by the load and road slope. When the rainfall intensity is less than 98 mm/h, there will be no surface runoff [14].

More importantly, there is an inevitable relationship between the viscoelastic parameters of a permeable asphalt mixture and temperature. With decreasing temperature, the viscoelastic parameters of the mixture gradually become elastic parameters. At the same time, the bulk modulus and shear modulus in the plastic model also gradually show obvious viscoelastic properties with the increase and decrease in temperature [15]. In terms of structure design, the thickness and type of base course are the key factors affecting the mechanical properties of a permeable asphalt pavement. At the same time, the coarse-grained stress-absorbing layer can effectively absorb stress and reduce the occurrence of reflective cracks [16,17]. In addition, compared with the water-free state in the asphalt pavement structure, the stress field and displacement field inside the asphalt pavement structure widen pavement cracks under the action of water and dynamic load, causing the cracks to expand greatly, but have no obvious effect on the shear expansion of the cracks [18].

In summary, the current research on permeable asphalt pavements mainly focuses on pavement permeability, porosity, road performance and the mechanical properties of materials. The research on mechanical properties is still at the stage of single-axle loads, and there is a lack of in-depth studies on the mechanical properties of permeable asphalt pavements under multi-field coupling. According to the composition characteristics and functional objectives of porous pavement materials, the service environment is relatively complex, making it necessary to analyze multi-physical fields such as water permeability, heat transfer and stress. Therefore, it is necessary to study the temperature effect and mechanical response of permeable asphalt pavement under the coupling of temperature and structure fields. From the perspective of the coupling of heat transfer and stress, the

cooling effect and mechanical response of permeable asphalt pavement were studied, and the mechanical responses based on temperature effect and standard axle load (dynamic and static load) were analyzed.

2. Materials and Methodology

2.1. Materials

Based on its different permeable layers and permeable ranges, the pavement structure can be divided into three types [19], as shown in Figure 1: surface permeable type (Type A), base permeable type (Type B), and full permeable type (Type C). Among these, Type A is a double-sided permeable layer, and the upper layer of the three composite structures is made of self-developed drainage SBS-modified asphalt concrete (OGFC-13) mixed with fibers. The structural form of the permeable asphalt pavement and the thickness of each structural layer are as shown in Table 1.

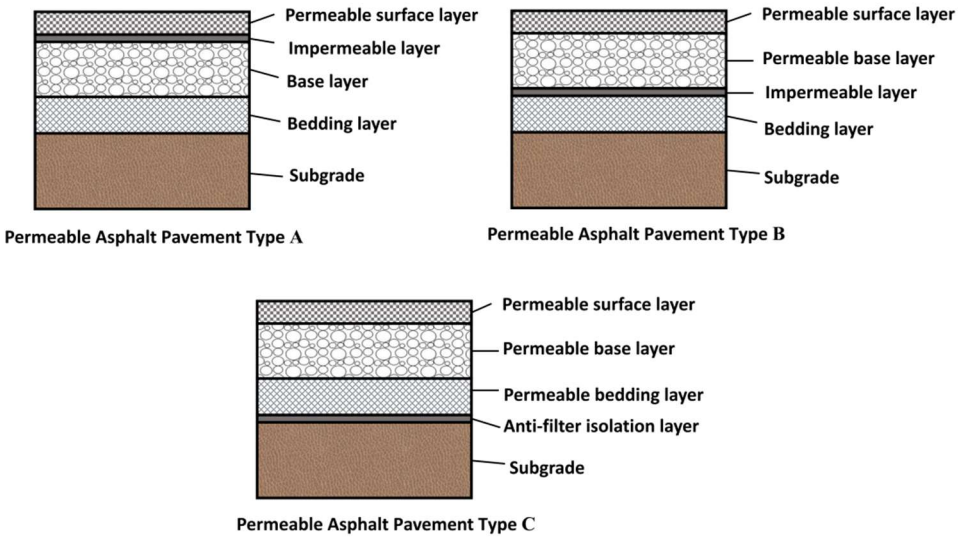

Figure 1. Permeable asphalt pavement structure types.

Table 1. Composite structure of permeable asphalt pavement.

STRUCTURAL LAYER	TYPE A	TYPE B	TYPE C	THICKNESS (CM)
TOP SURFACE COURSE	OGFC-13	OGFC-13	OGFC-13	12
THE FOLLOWING LAYER	ATPB-25	ATPB-25	ATPB-25	30
FOUNDATION COURSE	Water-stable gravel	Graded broken stone	Graded broken stone	25
BASE COURSE	Graded broken stone	Graded broken stone	Graded broken stone	20
SUBGRADE	Compacted soil	Compacted soil	Mild compacted soil	—

Note: OGFC is open graded friction course, ATPB is asphalt treated permeable base.

2.2. FEM Model

2.2.1. Basic Assumptions

Based on the theory of elastic layered systems, ANSYS (APDL19.2) was used to establish a numerical model to analyze the structural mechanics of a permeable asphalt pavement, and the actual solar radiation intensity was used as the heating condition to analyze and calculate the surface temperature of the permeable asphalt pavement. The following hypotheses were proposed.

(1) Basic assumptions of temperature field model

① Each structural layer of the permeable asphalt pavement was considered to be homogeneous and have a continuous material composition.

② The contact state, temperature and heat transfer between the structural layers were considered to be continuous, without thermal resistance, and the heat transfer interface effect between the layers was not considered.

③ The soil base surface was considered to be in a constant temperature state, and the geothermal effect on the temperature of the pavement structure was not considered.

④ The top surface of the model was the heating surface, and the other surfaces were adiabatic surfaces. The actual heat loss of the adiabatic surface and the external thermal convection process were not considered.

⑤ Only the effect of solar radiation was considered, while wind speed and other factors were not considered.

(2) Basic assumptions of mechanical model

① Each structural layer was considered to be a homogeneous and isotropic elastic material.

② The road surface was subjected to axisymmetric uniform vertical load, and the stress and strain at the infinite depth of the bottom layer and the horizontal infinite position were zero.

③ Stress, strain and displacement can be expressed by continuous functions of coordinates.

④ Structural weight was not considered.

2.2.2. Determination of Pavement Structure Parameters

In this study, ANSYS software (APDL 19.2) was used to analyze the mechanics of three kinds of permeable asphalt pavement, ignoring the instantaneous plastic deformation caused in the pavement structure during the fast-driving process of the vehicle. The size of the pavement structure model was 6000 mm × 3000 mm × 5000 mm, and SOLID 70 was selected as the temperature field analysis unit. After the analysis was completed, it was converted into the SOLID 185 unit for structural field analysis. All the units were eight-node three-dimensional hexahedral units. The grid was divided from fine to coarse, and the analysis area was encrypted.

In addition, the initial state of the pavement structure was assumed to be stress-free. The horizontal and vertical boundaries of the uppermost layer of pavement were unconstrained, and the bottom of soil foundation was completely fixed. The horizontal displacement of the left and right sides of the pavement structure model was set to 0, and the longitudinal displacement of the front and rear sides of the pavement structure model was set to 0.

2.2.3. Determination of Pavement Material Parameters

The values of material mechanical parameters and thermophysical parameters based on previous research results are shown in Tables 2 and 3. In fact, the material of permeable asphalt pavements is greatly affected by temperature, and the results analyzed without considering the influence of temperature on material parameters cannot accurately reveal the mechanical response characteristics of a permeable asphalt pavement structure [20]. Therefore, the influence of temperature change on the surface layer material parameters can be considered, and the change of other structural layer material parameters with temperature can be ignored [21].

Table 2. Mechanical parameters of pavement materials.

STRUCTURAL LAYER	MATERIAL	ELASTIC MODULUS (MPA)	POISSON RATIO (M)	DENSITY (KG/M3)
TOP SURFACE COURSE	OGFC-13	1400	0.25	2500
THE FOLLOWING LAYER	ATPB-25	800	0.35	2100
FOUNDATION COURSE	Water-stable gravel	1500	0.25	2300
BASE COURSE	Graded broken stone	500	0.35	2100
SUBGRADE	Soil	50	0.35	1850

Table 3. Values of thermal properties.

Structure Type	Heat Capacity (J/kg·°C)				Thermal Conductivity (W/m·°C)			
	Top Surface Course	The Following Layer	Foundation Course	Base Course	Top Surface Course	The Following Layer	Foundation Course	Base Course
A	800	800	600	800	0.6	0.6	1.1	0.8
B	800	800	800	800	0.6	0.6	0.8	0.8
C	800	800	800	800	0.6	0.6	0.8	0.8

(1) Elastic modulus

The functional relationship between elastic modulus and temperature load is as follows in Equation (1) [22].

$$\frac{E_T}{E_0} = 10^{0.01693(20-T)} \quad (1)$$

where T is the calculating temperature, °C, E_T is the elastic modulus at the calculated temperature, MPa, E_0 is the elastic modulus at standard temperature (20 °C), MPa.

(2) Poisson ratio

The values of the Poisson ratio of asphalt mixture at different temperatures in references are obtained [22,23]. The relationship between the Poisson ratio of an asphalt mixture and temperature is obtained by linear regression, as shown in Equation (2).

$$\mu_1(T) = 0.005 \times T + 0.15 \quad (2)$$

where $\mu_1(T)$ is the Poisson ratio of the asphalt mixture.

(3) Coefficient of linear expansion

The temperature linear expansion coefficient of an asphalt mixture can be expressed by Equation (3) [21].

$$\alpha_1(T) = 35.28e^{-\left(\frac{T+6.004}{36.07}\right)^2} \times 10^{-6} \quad (3)$$

where $\alpha_1(T)$ is the temperature linear expansion coefficient of asphalt layer at 1/°C.

2.2.4. Determination of Load Parameters

The tire contact area needs to be determined when the pavement structure is analyzed and simulated. It is assumed that the vehicle load is evenly distributed on the contact surface between the tire and the road surface, and the area of the contact surface is calculated according to the contact pressure value. In order to facilitate the simulation, the elliptical load is transformed into a rectangular load.

(1) Static load parameters

In the pavement design, a rectangular load was used in the structural mechanics calculations [24]. The rectangular load area was 0.8712 L × 0.6 L, and the standard axle load BZZ-100 was used in the calculation and analysis. The tire grounding equivalent rectangular side length is shown in Equations (4)–(6).

$$S = \frac{F}{P} \quad (4)$$

$$L = \sqrt{\frac{S}{0.5227}} \quad (5)$$

$$D = 1.5\sqrt{\frac{4S}{\pi}} \quad (6)$$

where S is the rectangular load area, m^2; L is the rail length of the driving direction, m; and D is center distance of two wheels, m.

According to the calculation results of Equations (4)–(6), the center distance of the two wheels was 0.32 m, and the adjusted distance was 31.98 cm. The rectangular side length of the single wheel was 0.157 m × 0.227 m, and the adjusted distance was 0.167 m × 0.213 m according to the actual situation. The clearance between the two wheels was 0.106 m. The calculation parameters of the standard axle load and the specific content of the rectangular load are shown in Table 4.

Table 4. Standard axle load calculation parameters.

STANDARD AXLE LOAD	BZZ-100	STANDARD AXLE LOAD	BZZ-100
STANDARD AXLE LOAD P (KN)	100	Single wheel transmission equivalent rectangular edge length L (cm)	16.7 × 21.3
TIRE GROUND PRESSURE P (MPA)	0.70	Center distance of two wheels (cm)	31.95

(2) Dynamic load parameters

The dynamic load was in the form of half sine [25]. According to the current pavement design specifications, P_{max} = 0.7 MPa, the equivalent radius of single wheel pressure transmission was 10.65 cm. The relationship between load and time is shown in Equation (7):

$$\begin{cases} P = P_{max} \times \sin(\frac{\pi}{T}t) & 0 \le t \le T \\ P = 0 & t > \mathrm{T} \end{cases} \quad (7)$$

The relationship between loading time and vehicle speed is shown in Equation (8).

$$T = 12\frac{R}{V} \quad (8)$$

where R is the equivalent circle radius of single wheel pressure transmission, cm; and V is the vehicle speed, km/h.

When the vehicle speed was 60 km/h, the load action time was 0.0767 s. From Equations (7) and (8), the change in load period is shown in Figure 2.

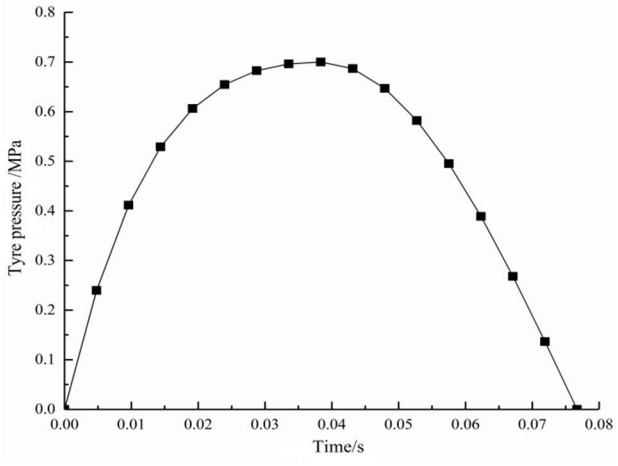

Figure 2. Diagram of load form.

(3) Temperature load parameters

The variation in daily solar radiation intensity in a certain area was taken as the daily solar radiation intensity on the road surface of the road structure. The results are shown in Figure 3. The absorption coefficient of the permeable asphalt pavement structure surface was set as 0.87 [17]. The analysis curve of temperature change with time during the 12 h

heating process for the three kinds of pavements is shown in Figure 4, which was applied as temperature load.

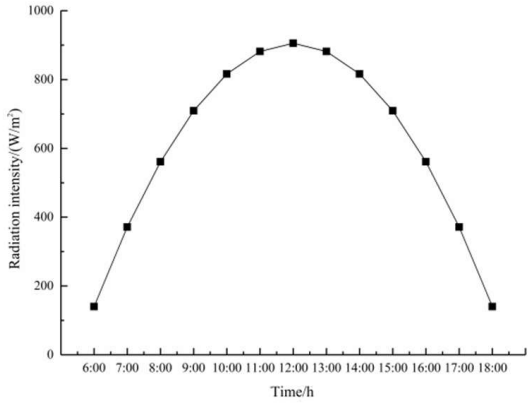

Figure 3. Diurnal variation curve of solar radiation intensity.

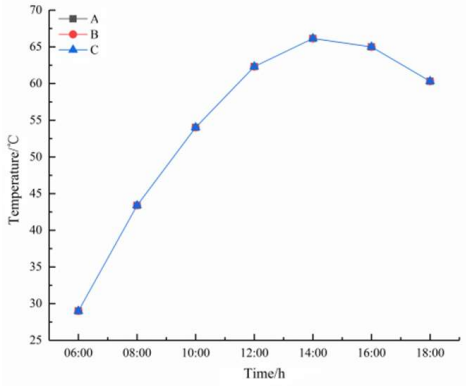

Figure 4. The 12 h heating curve of a permeable asphalt pavement.

2.3. Data Processing and Analysis

Technical specification for permeable asphalt pavement (CJJ/T 190-2012) [26] stipulates that the design of a pavement structure should take the deflection value of the pavement surface and the bending tensile stress at the bottom of structural layers as design indexes. The load mode of mechanical calculation using the theory of an elastic layered continuous system is a vertical uniform load, and the interlayer contact condition is completely continuous. According to the specification, the mechanical variation law of the permeable asphalt pavement structure was analyzed by the deflection value of the road surface, the flexural tensile stress and shear stress at the bottom of each structural layer.

2.3.1. Model Validity Analysis

When using finite element software for analysis, it is often necessary to verify the correctness of the model to ensure that the boundary conditions, mesh division and element type are reasonable. The calculation results in the relevant literature [27,28] are used as the reference to verify the correctness of the model. Due to differences in the simulation software or calculation accuracy, there will be some errors in the calculation results. Therefore, when conducting verification, if the relative error is within 10%, the model created is considered to be feasible [22]. The mechanical model verification and temperature field model verification are carried out, respectively. The modeling materials, load parameters and boundary conditions are the same as the existing research results, and the relevant parameters are shown in Tables 5 and 6.

Table 5. Material parameters of mechanical model structures.

STRUCTURAL TYPE	MATERIAL	THICKNESS (MM)	ELASTIC MODULUS (MPA)	POISSON RATIO (μ)	DENSITY (KG/M3)
TOP SURFACE COURSE	PAC-13	40	900	0.25	2100
THE FOLLOWING LAYER	PAC-16	60	850	0.25	2100
BASE LAYER	Cement stabilized macadam	200	1500	0.25	2300
PAVEMENT SUBBASE	Graded broken stone	150	500	0.35	2100
SUBGRADE	Soil	—	50	0.35	1850

Table 6. Material parameters of temperature field model structures.

STRUCTURAL TYPE	TOP SURFACE COURSE	THE FOLLOWING LAYER	BASE LAYER	PAVEMENT SUBBASE	SUBGRADE
MATERIAL	OGFC-13	ATPB	Graded broken stone	Graded broken stone	Soil
THICKNESS (MM)	100	200	200	300	500

2.3.2. Analysis of Mechanical Indexes with and without Temperature Effect

The three types of permeable asphalt pavement were analyzed with 12 h heating, and the pavement temperature calculation results at the peak time of pavement temperature were extracted as temperature conditions for the coupling field calculation. The surface deflection, compressive strain of the soil foundation top, tensile stress and shear stress of asphalt layer bottom were extracted and compared. The calculation time was 8 h, the pavement temperature was 66 °C, the static load was a standard axle load, and the dynamic load speed was 60 km/h.

2.3.3. Influence of Temperature Change on Mechanical Indexes

Firstly, the radiation intensity mentioned above was used as the temperature condition to calculate the temperature rise in the pavement structure for 12 h. Then, the temperature field calculation results were saved every 2 h from the initial time, and applied as the temperature load of the coupled field calculation. The temperature change was represented by the different time of the temperature rise calculation. The corresponding mechanical indexes were extracted and the time–mechanical index change curve was plotted to analyze the influence of temperature change. Among them, the static load was the standard axle load and the dynamic load speed was 60 km/h.

2.3.4. Influence of Vehicle Speed on Mechanical Properties of Permeable Asphalt Pavement

The finite element calculations for three kinds of permeable asphalt pavement were carried out under the same temperature condition as described in the above section, and the calculation results of each control index peak under dynamic load were extracted to analyze the influence of vehicle speed change on the main control indexes. The speed values were 40 km/h, 60 km/h, 80 km/h, 100 km/h, and 120 km/h.

3. Results and Discussion

3.1. Validity Analysis of Model

(1) Mechanical model validation analysis

The results for the deflection of the road surface and the compressive strain of the top surface of the soil foundation in the literature [24] were compared with the simulation results in this paper, as shown in Figure 5.

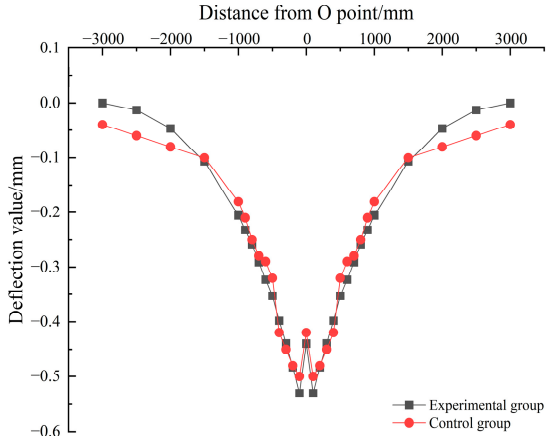

(**a**) Comparison of deflection value results

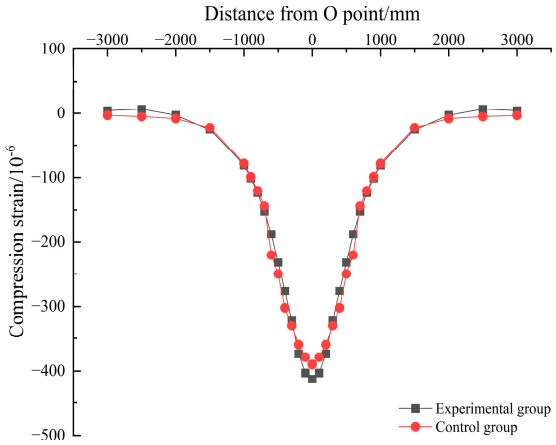

(**b**) Comparison of compressive strain results on top surface of soil foundation

Figure 5. Verification of the validity of the mechanical model.

It can be seen from Figure 5 that the calculation results of the deflection value of the finite element model and the compressive strain value of the top surface of the soil foundation in this paper are consistent with the results in the literature. In addition, the deflection value and the peak point of the compressive strain on the top surface of the soil foundation calculated in this paper are the same as those in the literature. The peak value of the surface deflection calculated in this paper is 0.53 mm, and the peak value of the compressive strain on the top surface of the soil foundation is 412 με, which are 6% and 5.6% larger, respectively, than those in the existing research results [24], which proves the rationality of the boundary conditions, mesh division and element type of the model.

(2) Temperature field model verification

The calculation results for the road surface temperature in the literature [27] were compared with the simulation results in this paper, as shown in Figure 6.

It can be seen from Figure 6 that the simulation results of this paper have the same change rule as the results of the existing research [27], and both increase with the increase in radiation intensity. However, between 6:00 and 10:00, the temperature calculation results of this paper are basically consistent with the temperature change curve in the literature results. After 10:00, the calculation results of this paper are different from those in the literature, but the difference is small. In this paper, the calculated temperature peak is 65.33 °C, which is only 1.81% larger than the existing research results, thus proving the effectiveness of the temperature field model in this paper.

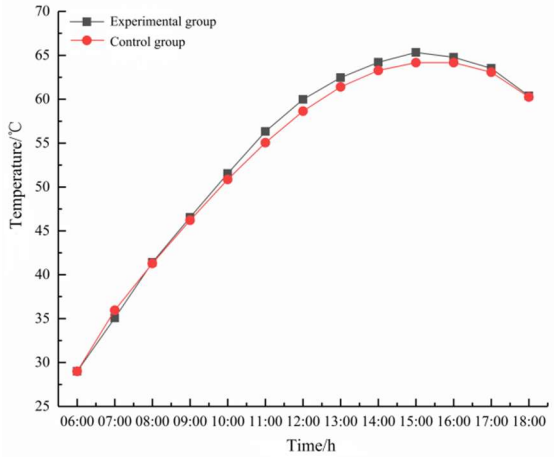

Figure 6. Verification of the validity of the temperature field model.

3.2. Analysis of Mechanical Indexes with and without Temperature Effect

3.2.1. Variation of Road Surface Deflection

It can be seen from Figure 7 that no matter whether there is temperature effect or not, the surface deflections of the three types of permeable asphalt pavements show half-sine changes under a half-sine dynamic load, while under a static load, the surface deflection value is constant. The surface deflections of the three types of pavement under a static load with a temperature effect are 0.56 mm, 0.61 mm and 0.71 mm, which are about 0.27 mm, 0.27 mm and 0.33 mm higher than the respective values under no temperature effect. The surface deflections under a dynamic load with temperature effect are 0.52 mm, 0.56 mm and 0.68 mm, which are about 0.24 mm, 0.24 mm and 0.31 mm higher than the respective values under no temperature effect. It can be seen that the peak values of the surface deflection values of the three types of pavements under dynamic load are smaller than those under static load. At the same time, due to the effect of temperature, the deflection values of the three types of pavements all increase to varying degrees, and the change in the type C structure is more prominent.

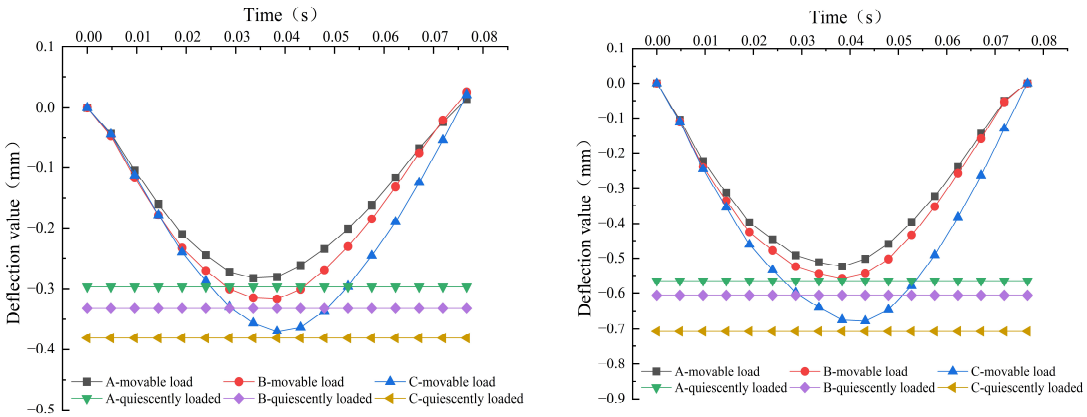

(**a**) No temperature effect (**b**) Temperature effect

Figure 7. Comparative analysis of road surface deflection.

3.2.2. Variation of Compressive Strain on Top of Soil Foundation

It can be seen from Figure 8 that whether there is temperature effect or not, the variations in the top surface compressive strain of the three kinds of permeable asphalt pavements under dynamic load are the same as those for road surface deflection, which show half-sine variation and are constant under static load. The values of peak compressive strain of the top surface of the soil foundation of the three types of pavements under static

load with temperature effect are 223 με, 246 με and 301 με, which are increased by about 30%, 28% and 38% compared with the respective values without temperature effect. The values of peak compressive strain of the top surface of the soil foundation under dynamic load with temperature effect are 208 με, 227 με and 286 με, which are increased by about 31%, 29% and 33% compared with the respective values without temperature effect. It can be seen that the peak values of the top surface compressive strain of the three types of pavements under static load are also greater than those under dynamic load. Moreover, due to the existence of the temperature effect, the compressive strain on the top surface of soil foundation has a large increase, which is similar to the road surface deflection, and the largest increase is still type C.

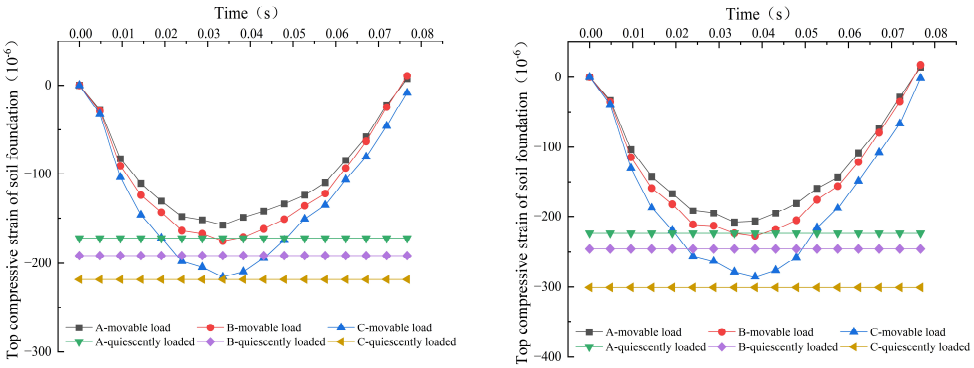

(**a**) No temperature effect (**b**) Temperature effect

Figure 8. Comparative analysis of compressive strain on top of soil foundation.

3.2.3. Shear Stress Variation of Top Surface Course

It can be seen from Figure 9 that the shear stresses at the bottom of the top surface course of the three types of permeable asphalt pavement show half-sine variation under dynamic load, and the value is fixed under static load. The peak values of the shear stress at the top surface course of the three kinds of pavements under dynamic load are less than the respective values under static load, but the differences are small. In addition, under the same conditions, the peak values of shear stress at the top layer and bottom of the three types of pavements under dynamic load and static load are about 0.10 MPa, 0.11 MPa and 0.12 MPa, respectively. However, these values increase to a certain extent under the action of temperature by about 46%, 39% and 38%, respectively. This phenomenon indicates that the existence of the temperature effect has a great influence on the shear stress of the top surface course of permeable asphalt pavements.

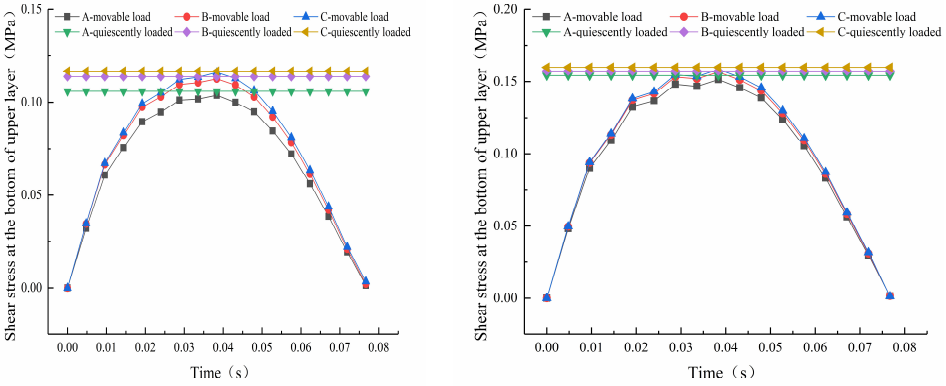

(**a**) No temperature effect (**b**) Temperature effect

Figure 9. Comparative analysis of shear stress at top surface course.

3.2.4. Variation of Tensile Stress at Bottom of Top Surface Course

It can be seen from Figure 10 that the tensile stresses at the bottom of the top surface course of the three types of permeable asphalt pavements show half-sine variation under dynamic load, and the value is fixed under static load. At the same time, as for the shear stress at the bottom of the top surface course, the peak values of the tensile stress at the bottom of the upper layer of the three types of pavements under dynamic load are smaller than those under static load, and the differences are not large. Under the same conditions, the peak values of tensile stress at bottom of the top surface course of the three types of pavements under dynamic load and static load are about 0.19 MPa, 0.19 MPa and 0.20 MPa, respectively, which are about 0.1 MPa higher than the respective values without temperature effect, which is consistent with the conclusion that the effect of high temperature on the increase in compressive stress is not significant in the existing research [28]. This also shows that the existence of the temperature effect also has a great influence on the tensile stress of the top surface course of permeable asphalt pavements.

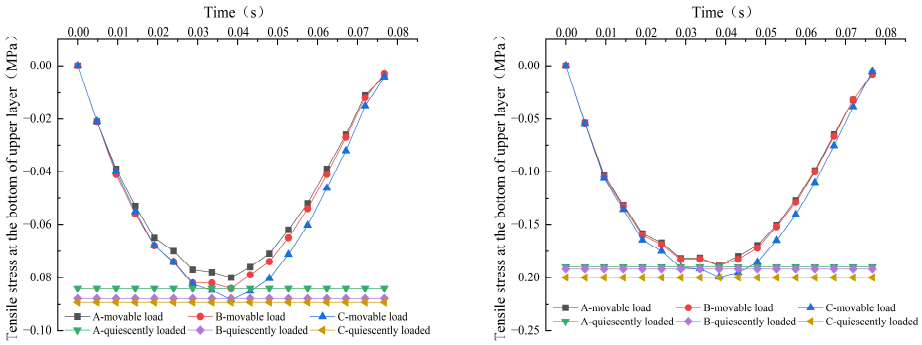

(**a**) No temperature effect (**b**) Temperature effect

Figure 10. Comparative analysis of tensile stress at bottom of top surface course.

3.3. Influence of Temperature Change on Mechanical Indexes

3.3.1. Influence on Road Surface Deflection

It can be seen in Figure 11 that under the action of dynamic load and static load, the surface deflection of the three types of permeable asphalt pavements has the same change rule with pavement temperature. The pavement temperature gradually increases from 6:00 to 14:00, and the deflection value at the surface load also continues to increase. The pavement temperature and deflection reach a peak at 14:00. Between 14:00 and 18:00, due to the decrease in pavement temperature, the deflection values of the load on the road surface begin to decrease. Comparing the road surface deflection values under static load and dynamic load, it can be found that at any time, the values for the same structure under static load are all greater than those under dynamic load, with C > B > A.

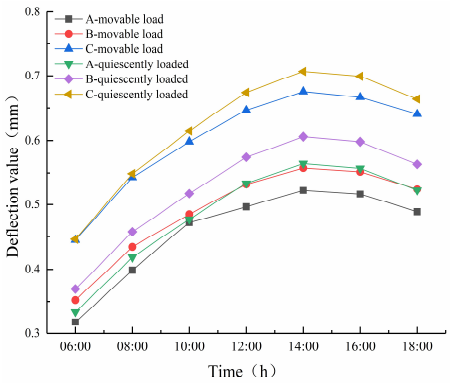

Figure 11. Influence of temperature change on road surface deflection.

3.3.2. Influence on Compressive Strain of Top Surface of Soil Foundation

It can be seen from Figure 12 that under both static and dynamic loads, the influence of temperature change on the compressive strain of soil foundation top surface of the three types of permeable asphalt pavements is different from that of road surface deflection. In the whole loading cycle, the top surface compressive strain of the three kinds of pavements increases with the increase in temperature, but the growth rate does not increase linearly with the increase in temperature, and there is no inflection point in the 12 h heating process. The top compressive strain of the three kinds of pavements can be seen as an obvious increase from 6:00 to 8:00. After 8:00, the increase is less obvious. This is because the soil foundation at the bottom of the structure is less affected by temperature, and the slight growth is mainly due to the small modulus of the soil foundation itself. This is the same as the influence of temperature on the compressive strain of the soil foundation top surface under the action of a standard axial load (static load) under the same conditions. It can also be seen from the figure that at any time, the compressive strain values of the soil foundation top surface of the three types of permeable asphalt pavements are C > B > A.

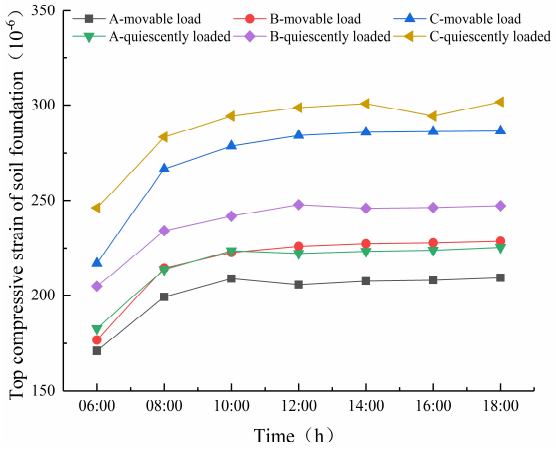

Figure 12. Influence of temperature change on the compressive strain of the top surface of the soil foundation.

3.3.3. Influence of Shear Stress on the Bottom of Top Surface Course

It can be seen from Figure 13 that during the heating process of 12 h, the shear stress at the bottom of the top surface course of the three types of permeable asphalt pavements is basically consistent with the change rule of surface deflection with temperature, and there is also an inflection point at 14:00. Between 6:00 and 14:00, the shear stress at the bottom of the top surface course of the three pavements increases gradually, and the values of shear stress reach a peak at 14:00. Then, the values of shear stress of the three pavements begin to decrease between 14: 00 and 18:00. Whether under static or dynamic load, the shear stress at the bottom of top surface course of the three pavements increases with the increase in temperature. At the same time, the shear stress values at the bottom of the type B and C pavements are basically equal in the whole cycle, while that of the type A pavement is smaller than the values for the B and C pavements. This observation is consistent with the findings of existing studies [20].

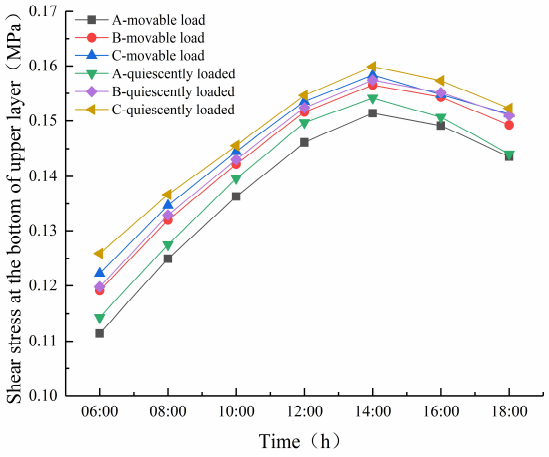

Figure 13. Influence of temperature change on shear stress on the bottom of the top surface course.

3.3.4. Influence on Tensile Stress at Bottom of the Top Surface Course

It can be seen from Figure 14 that in the 12 h heating process, the tensile stress and the shear stress at the bottom of top surface course of the three types of permeable asphalt pavements are the same, which is basically consistent with the rule of the surface deflection value changing with temperature, and the inflection point appears at 14:00. Before 14:00, the bottom tensile stress of the three pavements increases with the increase in pavement temperature. At 14:00, when the tensile stress at the bottom of the top surface course reaches a peak, the tensile stress at the bottom of the top surface course of the three pavements begins to decrease. In addition, it can be seen from Figure 14 that whether under static or dynamic load, the values of tensile stress at the bottom of the top surface course of the A and B pavements are basically equal in the whole cycle, while the tensile stress at the bottom of the top surface course of the type C pavement is greater than the respective values for A and B. In particular, the tensile stress at the bottom of the top surface course of the type C pavement under static load is significantly greater than that under other conditions.

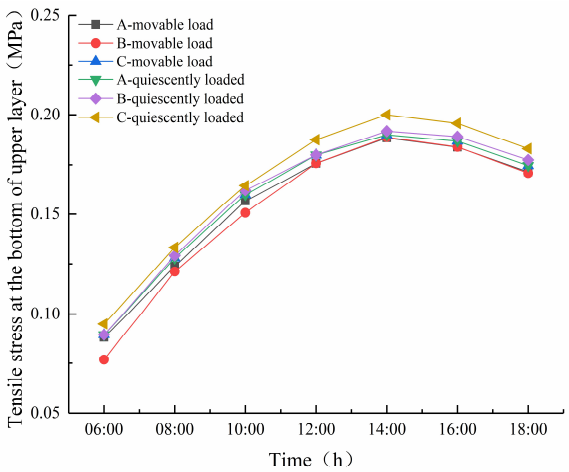

Figure 14. Influence of temperature change on tensile stress at bottom of the top surface course.

3.4. Influence of Speed Change on Mechanical Properties of Permeable Asphalt Pavement

3.4.1. Influence on Road Surface Deflection

Figure 15 shows that for the three types of pavement and under the action of dynamic load, the rule of surface deflection changes with speed is equal at the same time, regardless of the temperature effect. When the speed is 40–60 km/h, the deflection value increases with the increase in speed, reaches a peak at 60 km/h, and then decreases with further increases in speed. Comparing the road surface deflection under static load at the same

conditions, it can be seen that the peak value of road surface deflection under dynamic load is smaller than that under static load. In addition, for the three types of pavements, regardless of the temperature effect, the surface deflection values under the same load are C > B > A.

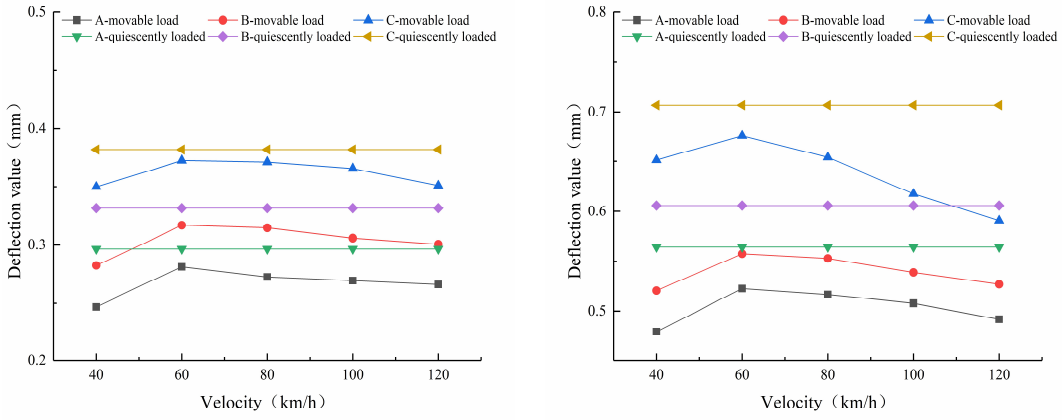

(**a**) No temperature effect (**b**) Temperature effect

Figure 15. Influence of speed change on road surface deflection.

3.4.2. Influence on Compressive Strain of Top Surface of Soil Foundation

It can be seen from Figure 16 that for the three types of pavements, the variation in compressive strain of the soil foundation top surface with speed is the same with or without temperature effect. When the load reaches a peak value (1/2T), the top compressive strain of the soil foundation increases from 40 km/h to 60 km/h without the temperature effect, but the change is not obvious. The difference between the temperature effect and the non-temperature effect condition is that there is no obvious fluctuation in the whole range of speed. When the speed is less than 60 km/h, it has a great influence on the compressive strain of the top surface of the soil foundation of the pavements without temperature effect. The degree of influence decreases with the increase in speed, and the influence of the speed change on the compressive strain of the top surface of the soil foundation of the pavement with temperature effect is small over the whole range. In addition, under the same conditions, the peak compressive strain of the soil foundation top surface under dynamic load is smaller than that under static load, which is the same pattern observed for the deflection value of the road surface.

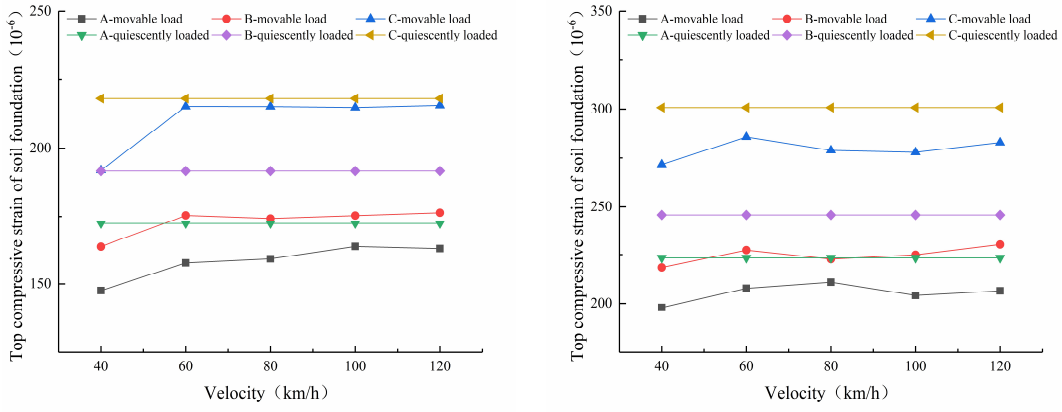

(**a**) No temperature effect (**b**) Temperature effect

Figure 16. Influence of speed change on compressive strain of the top surface of the soil foundation.

3.4.3. Influence of Shear Stress on the Bottom of the Top Surface Course

It can be seen from Figure 17 that with the increase in speed, the shear stress at the bottom of the top surface course of the three types of pavements either increases or decreases at different times. Whether the temperature effect exists or not, the changes in the shear stress at the bottom of the top surface course of these pavements are as follows: the shear stress values increase with increases in speed from 40 km/h to 60 km/h, decrease as the speed increases from 60 km/h to 80 km/h, and then increase with the speed. Therefore, whether there is temperature effect or not, the shear stress values at the bottom of the top surface course reach a maximum at the speed of 60 km/h and fluctuate between 40 km/h and 80 km/h.

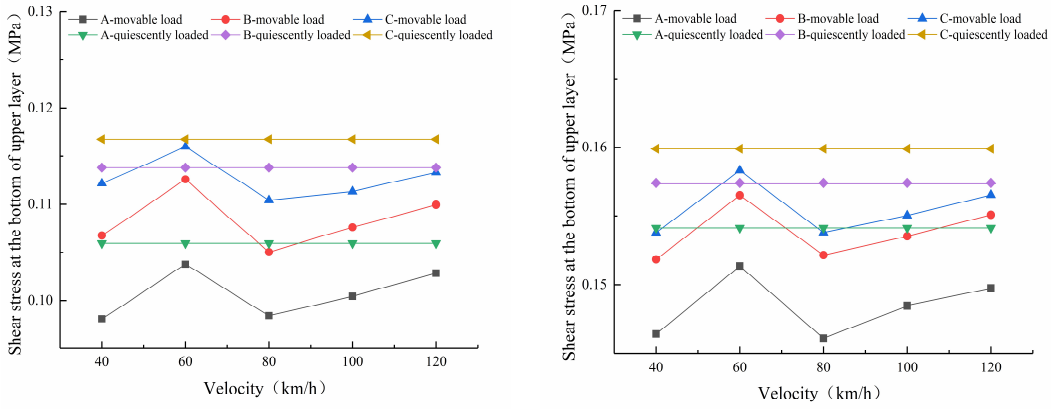

(**a**) No temperature effect (**b**) Temperature effect

Figure 17. Influence of speed change on shear stress on the bottom of the top surface course.

3.4.4. Influence on Tensile Stress at the Bottom of the Top Surface Course

It can be seen from Figure 18 that, as for the surface deflection and the compressive strain of the top surface of the soil foundation, the three pavements have the same law of tensile stress at the bottom of the upper layer, with or without the temperature effect, at the same time. Whether there is temperature effect or not, when the speed is 40–60 km/h, the tensile stress values at the bottom of the top surface course increase with increases in speed, reaching a peak at 60 km/h, and then decrease with further increases in speed. It can be seen that the speed of 60 km/h is the turning point of the tensile stress peak at the bottom of the entire top surface course at the peak load. In addition, under the same conditions, the peak tensile stress at the bottom of the top surface course under dynamic load is less than that under static load.

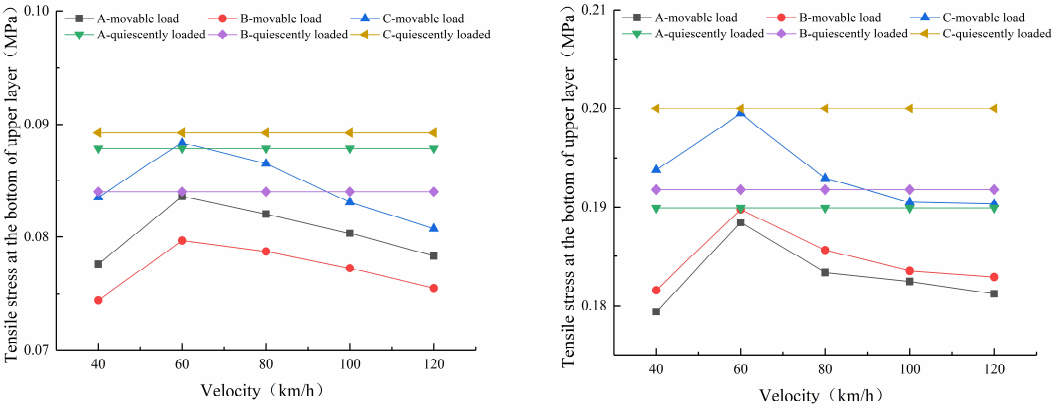

(**a**) No temperature effect (**b**) Temperature effect

Figure 18. Influence of speed change on tensile stress at the bottom of the top surface course.

4. Conclusions

(1) Regardless of whether there is a temperature effect, the peak values of the surface deflection, the compressive strain on the top surface of the soil base, the shear stress at the bottom of the upper layer, and the tensile stress at the bottom of the upper layer of the three types of permeable asphalt pavements under static load are all fixed values. Under the action of dynamic load, they all show a semi-sinusoidal change. The extreme value of each control index under dynamic load is about 10% smaller than the extreme value under static load. At the same time, the extreme values under temperature conditions are 28%–50% larger than the extreme values without temperature conditions.

(2) During the 12 h heating process of the three types of permeable asphalt pavements, regardless of the dynamic load or static load, the variation law of each control index with temperature is the same as that under static load. At the same time, the surface deflection, and the shear stress and tensile stress at the bottom of the upper layer are basically consistent with the variation law of the surface temperature. The peak value of each control index under dynamic load is smaller than that under static load.

(3) Here, we only consider the coupling analysis of standard axle load and solar radiation. The influence of the water factor should be examined in follow-up studies in water–heat–structure coupling analyses, which would allow the simulation calculation of permeable asphalt pavements to more closely approximate reality.

Author Contributions: Conceptualization, Z.L. and H.Z.; methodology, Y.L. and H.Z.; software, X.W.; validation, Y.L., X.W. and T.G.; investigation, Y.L.; data curation, Z.L.; writing—original draft preparation, Y.L. and X.W.; writing—review and editing, Y.L.; visualization, X.W. and Y.L.; supervision, Z.L.; project administration, Z.L.; funding acquisition, Z.L. All authors have read and agreed to the published version of the manuscript.

Funding: This work was supported by Key R&D and Promotion of Special Scientific and Technological Research Projects of Henan Province: [Grant Number 182102210061, 212102310089]; Key Scientific Research Projects of Colleges and Universities in Henan Province in 2021: Study on pavement performance of cotton straw cellulose modified asphalt [Grant Number 21A580004].

Institutional Review Board Statement: Not applicable.

Informed Consent Statement: Not applicable.

Data Availability Statement: Some or all data, models, or code that support the findings of this study are available from the corresponding author upon reasonable request.

Conflicts of Interest: The authors declare no conflict of interest.

References

1. Gupta, A.; Rodriguez-Hernandez, J.; Castro-Fresno, D. Incorporation of additives and fibers in porous asphalt mixtures: A review. *Materials* **2019**, *12*, 3156. [CrossRef] [PubMed]
2. Garcia, E.S.; Thives, L.P.; Ghisi, E.; Antunes, L.N. Analysis of permeability reduction in drainage asphalt mixtures due to decrease in void volume. *J. Clean. Prod.* **2020**, *248*, 119292. [CrossRef]
3. Chen, C. New solution to the dilemma, urban water culture in Henan Province and its value in the construction of sponge city. *J. North China Univ. Water Resour. Electr. Power (Soc. Sci. Ed.)* **2019**, *35*, 1–6.
4. Zhang, Y.; Xu, Y. Technical Requirements for Structures and Materials of Permeable Asphalt Pavement. *Urban Bridges Flood Control.* **2019**, *4*, 51–54+9–10. [CrossRef]
5. Wang, X.; Gu, X.; Dong, Q.; Wu, J.; Jiang, J. Evaluation of permanent deformation of multilayer porous asphalt courses using an advanced multiply-repeated load test. *Constr. Build. Mater.* **2018**, *160*, 19–29. [CrossRef]
6. Jiang, W.; Sha, A.; Xiao, J. Selection of gradation ratio of porous asphalt mixture based on discrete element method. *J. Jilin Univ. (Eng. Ed.)* **2011**, *41*, 68–72.
7. Liu, B. Study on Road Performance Improvement of Urban Road Permeable Asphalt Pavement. Ph.D. Thesis, Southeast University, Nanjing, China, 2018.
8. Kusumawardani, D.M.; Wong, Y.D. Evaluation of aggregate gradation on aggregate packing in porous asphalt mixture (PAM) by 3D numerical modelling and laboratory measurements. *Constr. Build. Mater.* **2020**, *246*, 118414. [CrossRef]
9. Li, Z.; Chen, Y.; Sun, K. Thermal aging performance of porous asphalt mixture. *J. Chang'an Univ. (Nat. Sci. Ed.)* **2014**, *34*, 41–46.

10. Jiang, Y.; Gao, B.; Yang, Y.; Wu, J.; Wang, G. Research on typical permeable pavement model based on sponge city system. *J. Chongqing Jiaotong Univ. (Nat. Sci. Ed.)* **2019**, *38*, 42–47.
11. Hu, L.; Yun, D.; Yang, Z. Research on macro-structural characteristics of open-graded asphalt wear layer and its skid resistance under rainfall conditions. *Mater. Introd.* **2017**, *31*, 113–117+134.
12. Feng, Y.; Wang, W.; Li, J.; Li, P.; Guan, P. Experimental study on runoff coefficient of permeable road. *Water Conserv. Hydropower Technol.* **2019**, *50*, 27–35.
13. Tan, S.A.; Fwa, T.F.; Chai, K.C. Drainage considerations for porous asphalt surface course design. *Transp. Res. Rec.* **2004**, *1868*, 142–149. [CrossRef]
14. Xu, X.; Qin, H.; Zhuo, W. Study on the influence of permeable concrete pavement on rainwater runoff. *Highw. Eng.* **2019**, *44*, 135–139.
15. Yi, J.; Feng, D. Viscoelastic-plastic damage model of porous asphalt mixture. *J. Harbin Inst. Technol.* **2014**, *46*, 66–71.
16. Pang, Z.; Meng, X. Structural optimization scheme of permeable asphalt pavement based on finite element analysis. *Transp. Res.* **2018**, *4*, 69–76.
17. Deng, N.; Wu, K.; Huang, W.; Deng, Q. Coarse-grained stress absorbing layer pavement structure design and finite element analysis. *Sci. Technol. Eng.* **2019**, *19*, 316–321.
18. Huang, L.; Wu, W.; Shen, Q. Hydrodynamic pressure effect analysis of crack propagation in permeable asphalt pavement. *Highw. Eng.* **2019**, *44*, 181–185.
19. Ning, F. Design and Application of Permeable Asphalt Pavement Gravel Base Mixture. Master's thesis, Changsha University of Science and Technology, Changsha, China, 2019.
20. Wang, X. Research on Dynamic Response Characteristics of Permeable Asphalt Pavement under Multi-Field Coupling. Master's thesis, Shenyang Jianzhu University, Shenyang, China, 2018.
21. Luo, S. Study on the Disease Environment and Multi-Field Coupling Effect of Asphalt Pavement in High Temperature and Rainy Area. Ph.D. Thesis, Central South University, Changsha, China, 2012.
22. He, J. Mechanical Mechanism Analysis of Rutting Formation of Urban Asphalt Pavement under Temperature Field. Master's Thesis, Central South University, Changsha, China, 2014.
23. Chen, Y. Research on Disease Prevention and Control Technology of Asphalt Pavement on Long and Large Longitudinal Slope. Ph.D. Thesis, Chang'an University, Xi'an, China, 2011.
24. Du, W. Composition Design and Application Research of Permeable Asphalt Mixture. Master's Thesis, Beijing Jiaotong University, Beijing, China, 2019.
25. Wang, L.; Shan, C.; Zheng, C. Response Characteristics of Inverted-base Asphalt Pavement Structure in Cold Area under Multi-axle Loads. *Environ. Earth Sci. Res. J.* **2020**, *7*, 141. [CrossRef]
26. *CJJ/T 190-2012*; Technical Specification for Permeable Asphalt Pavement. China Building Industry Press: Beijing, China, 2012.
27. Tian, Y. Study on Water Holding Behavior and Cooling Effect of Urban Road Permeable Asphalt Pavement. Master's Thesis, Chang'an University, Xi'an, China, 2019.
28. Yang, Z. Mechanical response analysis of asphalt pavement structure under high temperature and heavy load. *Road Traffic Technol.* **2020**, *36*, 20–26.